Drop Size and Drop Size Distribution Measurements by Image Analysis

J. Blaisot

Drop Size and Drop Size Distribution Measurements by Image Analysis

J. B. Blaisot
CORIA UMR 6614, University of Rouen, France
blaisot@coria.fr

Abstract

One important issue in drop sizing by image analysis is the determination of the contour of the drops. The grey level corresponding to this contour strongly depends on the degree of focusing of a drop. This grey level is determined from an imaging model based on Fourier optics formalism. The presented method allows estimating the correct contour of a focused or of an out-of-focus droplet, for a large range of sizes. A size-independent criterion for the selection of drops accordingly to their position relative to the focus plane is also presented. This criterion is based on the estimation of the PSF width. The criterion is used to select drops within a controlled range of out-of-focus positions, which is necessary for the determination of drop size distributions in spray applications. The method is applied to calibrated objects to control the method accuracy. Sources of sizing errors are evaluated and techniques to enhance the sizing procedure and to deal with overlapped images are presented.

Introduction

Drops size distribution is a fundamental property of a spray and represents one of the main objectives of the design of an atomizer. Many attentions have been paid to develop drop sizing techniques and today image-based drop sizing techniques benefit from a renewed interest. The main drawback comes from the depth-of-field (DOF) of the system, i.e. images of the drops are not always focused. In addition, for the determination of the drop size probability density function (PDF) of a spray, the drops must be counted in a given control volume. So a criterion is needed to sort the droplets accounting for their distance from focus plane.

Most 'in-focus' criterion are either based on the grey level gradient at the particle boundaries [1-5] or on the contrast between the particle and the background [6-7]. These techniques aim to select best focused droplets in the image, meaning that drops located within a certain DOF tolerance are selected. Most of the techniques led to the determination of a sample volume that increases with the drop size, thus requiring weighting corrections of the drop size distribution, as shown by Ow & Crane [8]. The main drawbacks of these approaches are the droplet rejection rate which can be relatively high and the overestimation of the biggest droplets population, small droplets being more concerned by out-of-focus than the bigger ones.

An imaging system is optically characterized by its Point Spread Function (PSF) which corresponds to the optical image of an infinitely small object point. Digital image capturing systems can be classified in two categories: Pixel Limited (PL) systems and Optics Limited (OL) systems. An optimum is usually wanted by adjusting the PSF width to the pixel size (PL systems). For an OL system, the minimum size of an imaged point covers more than one pixel on the detector plane. This could be seen as a badly adapted system but in fact it allows the PSF width to be measured on the image. This measure is used here for the DOF criterion. It can be noted that miniaturization of image devices bring chips with increasingly small pixel size, offering better conditions to setup an OL system.

The measurement of droplet size is based on the determination of the particle contour. The criterion for the choice of the contour pixels at the particle boundary is usually based on grey level or on grey level gradient. Some authors [1, 3, 8] define a threshold level relative to the maximum grey level in the image but diameters measured on defocused droplets tend to decrease with out-of-focus, due to the decrease of contrast with defocus. Other authors [4, 9] used a criterion on the maximum grey level gradient in the image contour. However, Nishino et al [9] found that diameters tend to be overestimated for small out-of-focus particles, whereas they observed the opposite trend for the biggest particles. Fdida & Blaisot [10] proposed a method using a relative grey level value set at 61% of the image grey level amplitude for the determination of the contour. A correction of the raw measurement based on an imaging model is applied for in-focus or out-of-focus drop diameter estimation. This method has been successfully compared to diffraction and phase-Doppler interference techniques in application to fuel sprays [11, 12].

A new criterion for the determination of the drop contour is proposed here based on the recent developments made by the author on the imaging model for application to spray sizing and drop size distribution measurements. The principle of the model is recalled and the drop sizing procedure based on the new criterion is explained.

Practical application issues are addressed, particularly the drop size range, the measurement volume depth and the treatment of signal noise. The problem of image overlap is also addressed.

Imaging model

As image is a signal particularly well adapted to human perception, it is often falsely considered that raw data from an image can deliver quantitative information on the imaged object without needing any underlying physical model. Indeed, a 'simple' image analysis can be used to localize object boundaries in a natural scene and this is particularly true for a PL configuration. However, for a precise determination of the contour of a drop on a spray image it is necessary to evaluate the effect of the optical system performances in the image formation. The optical system is modeled by its PSF which can be considered as the response of the system to an infinitely small object source. Optical systems under consideration belong to the OL category. Indeed, we aim at precisely measuring drop sizes over a relatively large and controlled DOF, using a DOF criterion based on the measurement of the width of the PSF.

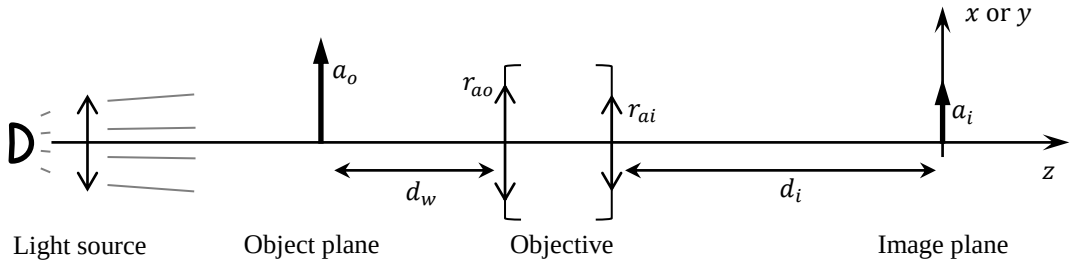

Figure 1 Optical arrangement of the imaging system. Relevant characteristics of the objective are indicated on the figure

Optical arrangement

To setup an imaging system for a drop sizing application, a backlight configuration is required. Additionally, the light source must be collimated and aligned with the optical axis of the objective. Using collimated or quasi-collimated light tends to promote forward light scattering near the axis direction. This helps in obtaining images with a better contrast and also tends to improve DOF. The relevant characteristics of the imaging system shown in figure 1 are the working distance d_w, the entrance and exit pupil aperture radii r_{ao} and r_{ai}, the lateral magnification γ_t and the imaging distance d_i. Another important characteristic is the pixel size p_i or the equivalent pixel size $p_o = p_i/\gamma_t$ expressed in the object plane. Working distance, imaging distance and magnification are linked together ($\gamma_t = d_i/d_w$ for thin lens approximation) and are experimentally fixed by the choice of the objective and the magnification. The magnification depends on the application and must be set to enable measurement of the smallest droplets in a spray. Magnifications used for fuel injection spray applications range from 0.1 for large sprays (0.1 – 5 mm) [2] up to 10 for fine sprays (5 – 100 µm) [3, 11, 12]. The aperture setting is a tradeoff between DOF and background image illumination. Low aperture is needed for large DOF but high aperture is necessary to reach adequate signal-to-noise ratio. This last point is determinant since the energy delivered by the light source can rarely be adjusted. Thus, the aperture must be kept as closed as possible since high aperture not only implies a DOF reduction but also a reduction of the PSF width for a diffraction-limited system. This is particularly the case for microscope-like objectives. Thus a change from OL to PL configuration can occur. However, for photographic objectives, larger aperture can result in a larger PSF, due to geometric aberrations, particularly the spherical aberration that is proportional to the third power of r_{ao} [10]. For a telecentric objective, Fdida and Blaisot [10] showed that a balance between aberration and diffraction limitation can be reached, resulting in a minimum PSF width that remains constant whatever the aperture setting.

Point Spread Function

For a diffraction-limited optical system of circular aperture under monochromatic illumination, the PSF is given by

$$PSF_{dl}(r;\alpha_\lambda) = s_{dl}\left(\frac{J_1(\alpha_\lambda r)}{\alpha_\lambda r}\right)^2 \quad (1)$$

where s_{dl} is a parameter depending on the wavelength λ, $\alpha_\lambda = 2\pi r_{ai}/\lambda d_i$ and $r = \sqrt{x^2+y^2}$ is the radial coordinate in the image plane. Considering the case of non-coherent polychromatic light and the contribution of geometric aberrations, Pentland [13] proposed to model the PSF by a Gaussian function:

$$PSF(r) = s_0 \exp\left(-\frac{2r^2}{\chi^2}\right) \quad (2)$$

where χ is the PSF half-width and s_0 is a normalization coefficient. The PSF width is minimal in the focus plane and increases with out-of-focus due to the increase of out-of-focus aberration. It is supposed that χ does not depend on the image plane coordinates (x, y), i.e. there is no spatial variation of the optical aberrations of the imaging system in the plane (x, y), and so the PSF half-width χ is considered to be a function of z only. This can be verified in the calibration needed for drop size applications, which consists in measuring $\chi(z)$ [10].

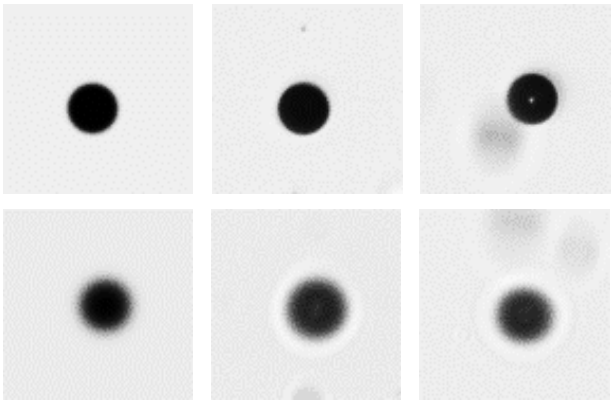

Figure 2 Theoretical and experimental normalized images: left column: images obtained by the model; middle column: image of a calibrated disc; right column: image of a droplet. Objects are 60µm in diameter. Upper row: focused position (2χ = 18 µm), Lower row: out-of-focus position (2χ = 40 µm).

Image formation

As mentioned before, we do particularly pay attention to the edge of droplet images as we are interested in the determination of the size and also of the shape of the drops. Liquid droplets in a spray are refractive objects but refraction effects on the image edge are limited here as can be seen in figure 2. Indeed, rigorous generalized Lorenz-Mie theory (GLMT) and PSF approaches are very similar on the very edge of the image profile [15]. Images of liquid droplets or opaque discs are thus very similar and this is particularly the case when the source is collimated. There is however a brighter spot in the center of the droplet image, where the refracted component of the light near the axis is prevailing [16].This difference is not restrictive here as only the outline of the image profile is considered. Thus, droplets are modeled as opaque or slightly transmitting objects without taking into account refraction in the image formation.

The PSF approach is based on Fourier optics formalism [17].The illumination distribution in the image plane $i(x,y)$ is expressed by the convolution product of the irradiance distribution in the object plane $o(x,y)$ and the PSF of the imaging system $PSF(x,y)$:

$$i(x,y) = o(x,y) \otimes PSF(x,y) \tag{3}$$

The object function $o(x,y)$ for a circular transmitting object of radius a_o is expressed by:

$$o(x,y) = 1 - (1-\tau)\,\Pi\left(\frac{r}{2|\gamma_t|a_o}\right) \tag{4}$$

where τ is the contrast coefficient characterizing the fraction of transmitted light ($0 < \tau < 1$, $\tau = 0$ for a perfectly opaque object) and $\Pi(t)$ is the rectangle function defined by:

$$\Pi(t) = \begin{cases} 1 & \text{for } |r| < 0.5, \\ 0 & \text{otherwise} \end{cases} \tag{5}$$

Introducing equations (2) and (4) into (3) and converting to circular coordinates yields equation (6):

$$\tilde{\imath}(\tilde{r}) = 1 - 2(1-\tau)\, e^{-\tilde{r}^2} \int_0^{\tilde{a}} \rho\, e^{-\rho^2}\, I_0(2\tilde{r}\rho)\; d\rho \tag{6}$$

The normalized illumination radial-profile $\tilde{\imath}(\tilde{r})$ represents the fraction of light transmitted to the image plane at a given dimensionless radial coordinate $\tilde{r} = \sqrt{2}\,r/\chi$. The image profile is controlled by two parameters, namely τ and $\tilde{a} = \sqrt{2}\,a_i/\chi$. The contrast coefficient τ controls the minimum level in the image, but not the profile shape. The dimensionless object radius $\tilde{a}$ controls blur effect and thus the shape of the image profile [10]. For large $\tilde{a}$, the profile is close to a U-shape.

For a given object radius, $\tilde{a}$ is maximum when the PSF width is minimum, i.e. when the object is in-focus. As object becomes more and more out-of-focus, PSF half-width χ increases and $\tilde{a}$ tends towards 0. For small $\tilde{a}$, the image presents a V-shape as in figure 3. It must be remarked also that for a

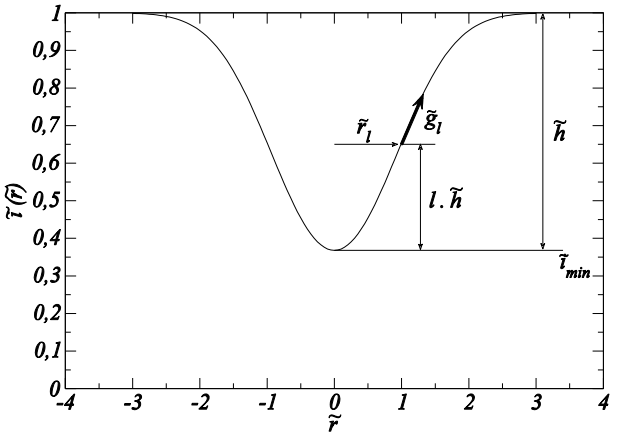

Figure 3 Image profile and parameters definition.

given imaging system, a small focused object and a big defocused object can have the same dimensionless radius $\tilde{a}$ and thus the same profile shape.

Image parameters

Relevant parameters for drop sizing are determined from the image profile. As mentioned before, a particular attention is given to the edges of the profile. Reference levels are first determined. Normalized profile possesses a maximum value ($\tilde{\imath}_{max} = 1$) and a minimum value ($\tilde{\imath}_{min} = 1 - (1-\tau)\left(1 - e^{-\tilde{a}^2}\right)$) that define the profile height $\tilde{h} = \tilde{\imath}_{max} - \tilde{\imath}_{min}$ and the image contrast $C = \tilde{h}/(\tilde{\imath}_{max} + \tilde{\imath}_{\min})$. As can be seen in figure 3, for every relative level l $(0 < l < 1)$, a reference level $\tilde{\imath}_l = \tilde{\imath}_{min} + l \cdot \tilde{h}$ and a reference radial coordinate $\tilde{r}_l$ associated to this reference level can be defined. The reference coordinate and level are related by an implicit relation ($\tilde{\imath}(\tilde{r}_l) = \tilde{\imath}_l$) expressed in equation (7):

$$e^{-\tilde{r}_l^2} \int_0^{\tilde{a}} \rho\, e^{-\rho^2}\, I_0(2\tilde{r}_l\rho)\, d\rho = (1-l) \int_0^{\tilde{a}} \rho\, e^{-\rho^2}\, d\rho \qquad (7)$$

It can be deduced from this equation that the reference coordinate $\tilde{r}_l$ does not depend on the contrast coefficient. The variation of $\tilde{r}_l$ as a function of $\tilde{a}$ is shown in figure 4 for relative level $l = 0.50$. When $\tilde{a}$ is large enough ($\tilde{a} > 1.5$) the reference radius $\tilde{r}_l$ increases linearly with the object width. For $\tilde{a} \longrightarrow 0$, $\tilde{r}_l$ tends to the half-width of the PSF at the relative level $(1-l)$ (see equation 7). It can be remarked that identity $\tilde{r}_l = \tilde{a}$ is reached for only one value of $\tilde{a}$.

The contrast C is bounded between 0 and 1. The maximum contrast is reached by the biggest objects in a sample. For perfectly opaque objects $C_{max} = 1$ but the effective maximum value (whatever the object size) depends on the contrast coefficient τ, i.e. $C_{max} = \frac{1-\tau}{1+\tau}$. The reciprocal relation $\tau = \frac{1-C_{max}}{1+C_{max}}$ is used for the determination of τ in spray applications. A normalized contrast C_0 whose maximum value is equal to 1 even for non-perfectly opaque objects is thus introduced:

$$C_0 = \frac{C}{(1-\tau)(1+C) - C} \qquad (8)$$

The variation of the normalized contrast is shown in figure 5 as a function of dimensionless object radius $\tilde{a}$. The contrast tends to zero for very small objects. As soon as the object width is around twice the PSF width, the contrast reaches its maximum value. It is the reason why the contrast cannot be used as a focus criterion (i.e. large objects have their contrast maximum whatever their focus level).

The dimensionless illumination gradient $\tilde{g}_l$ at the profile edge (relative level $\tilde{r}_l$) is introduced to characterize the profile edge and to define a focus criterion:

$$\tilde{g}_l = \frac{\partial \tilde{\imath}}{\partial \tilde{r}}\Big)_{\tilde{r}=\tilde{r}_l} = 4(1-\tau)e^{-\tilde{r}_l^2}\left[\tilde{r}_l \int_0^{\tilde{a}} \rho\, e^{-\rho^2}\, I_0(2\tilde{r}_l\rho)\, d\rho - \int_0^{\tilde{a}} \rho^2\, e^{-\rho^2}\, I_1(2\tilde{r}_l\rho)\, d\rho\right] \qquad (9)$$

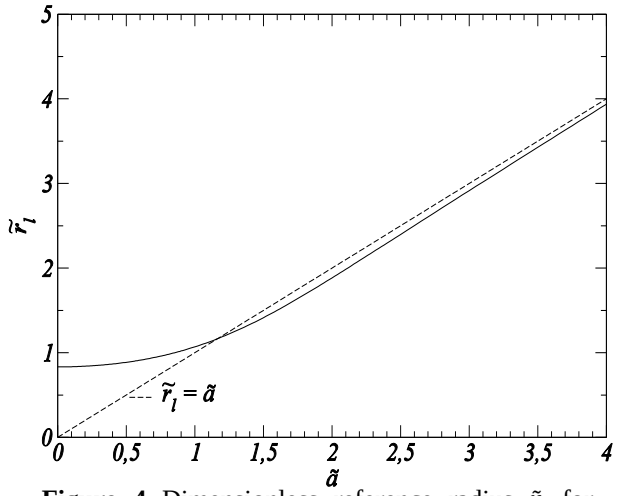

Figure 4 Dimensionless reference radius $\tilde{r}_l$ for relative level $l = 0.50$ as a function of dimensionless object radius $\tilde{a}$. Identity $\tilde{r}_l = \tilde{a}$ is also plotted.

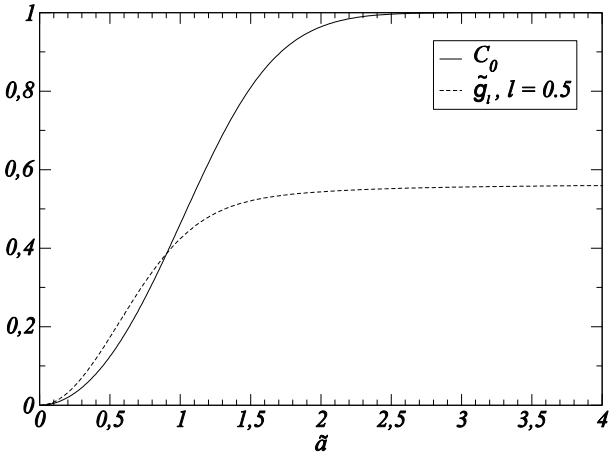

Figure 5 Normalized contrast C_0 and dimensionless grey level gradient for $l = 0.50$ and $\tau = 0$ as a function of dimensionless object radius $\tilde{a}$.

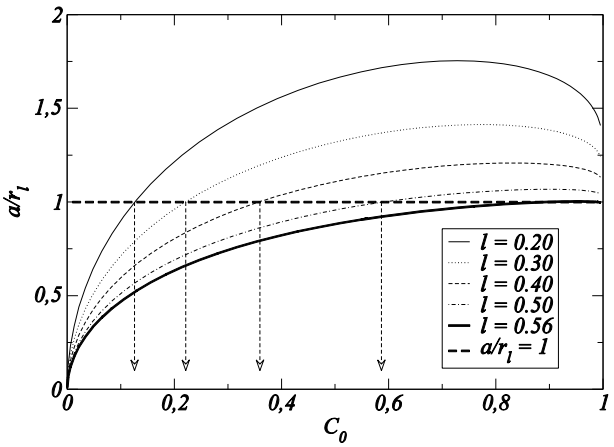

Figure 6 $a/r_l = p(C_0, l)$ for relative levels $l = (0.20: 0.30: 0.40: 0.50: 0.56)$.

The variation of the gradient is shown in figure 5 for the relative level $l = 0.50$. As seen above, for $\tilde{a} \longrightarrow 0$ the image profile is flattened, implying that gradient becomes null. For large value of the dimensionless object radius, the gradient tends to the limit value $1/\sqrt{\pi} \simeq 0.56$. This limit corresponds to the slope of the image of an optical edge [10]. The gradient is expressed here relatively to the dimensionless coordinate $\tilde{r} = \sqrt{2}\, r/\chi$. Even if a limit is reached for large objects (as for normalized contrast C_0), this limit just indicates that the gradient is only depending on PSF half-width χ. Thus, $\tilde{g}_l$ is used to measure χ and to derive the focus selection criterion (see below).

Sizing method criteria

Drop sizing criterion

The relative level that must be used to measure the object radius depends on the focus level. Indeed, as seen in figure 4, $\tilde{r}_l = \tilde{a}$ is reached for only one value $\tilde{a}$ for a given relative level l. The sizing criterion defines this particular relative level, noted l^*, by the implicit relation $\tilde{a}/\tilde{r}_{l^*} = 1$. It must be remarked here that $\tilde{a}/\tilde{r}_l = a/r_l$, and that C_0 is a monotonic function of $\tilde{a}$ (see figure 5). Thus, $\tilde{a}$ can be replaced by C_0 to derive the relation between a/r_l and C_0 shown in figure 6. This way, a direct relation $a/r_l = p(C_0, l)$ is obtained in which the unknown χ is eliminated. The sizing criterion consists in determining for each C_0 value, the relative level l^* giving $p(C_0, l^*) = 1$. This criterion is shown in figure 7. In applications to spray sizing, drop radii are thus determined on experimental normalized images from the measurement of C_0 and r_{l^*} (see Practical application section below).

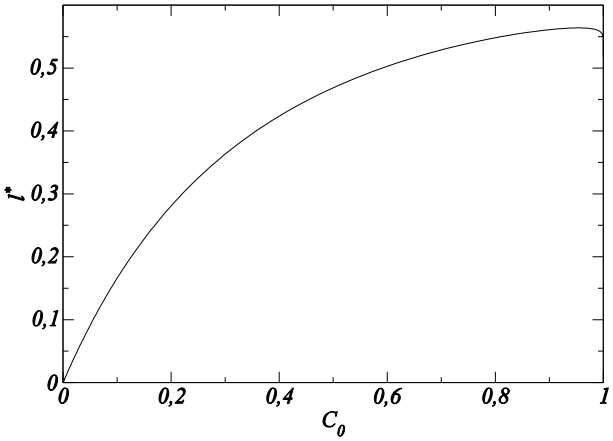

Figure 7 Sizing criterion giving the relative level of measurement l^* as a function of the normalized contrast C_0.

Focus selection criterion

The focus selection criterion is based on the measurement of the PSF half-width χ. The relation between the dimensionless gradient $\tilde{g}_l$ and the dimensionless object radius $\tilde{a}$ shown in figure 5 is turned into a relation between $\tilde{g}_l$ and C_0 for the reason already mentioned that C_0 is a monotonic function of $\tilde{a}$. The resulting relation $\tilde{g}_l = q(C_0, l)$ is shown in figure 8 for several relative levels. As grey level gradients are experimentally determined from a finite difference between grey levels, a high grey level gradient is more accurately measured on experimental images. Highest gradient is obtained around mid-level $l = 0.50$, for almost every image contrast. Experimental gradient $g_{0.50}$ at relative level $l = 0.50$ is thus measured on normalized images. The PSF half-width is then determined by identifying the two gradients, i.e. $\tilde{g}_{0.50} = \frac{\chi}{\sqrt{2}} g_{0.50}$. This way, χ is determined independently from the measurement of the drop diameter. The focus selection criterion that does not depend on the object size is simply expressed as a maximum acceptable value for χ, i.e. $\chi < \chi_{max}$.

Practical application

Sizing procedure applied to calibrated discs

Calibrated opaque discs are used as test objects to estimate the accuracy of the sizing procedure. These discs are placed in the field of view and translated along the optical axis z over a wide range of out-of-focus positions. In order to determine the normalized contrast for each image, the contrast coefficient τ is determined from $\tau = \frac{1 - C_{max}}{1 + C_{max}}$, where C_{max} is measured on the largest disc. A very low value is actually found ($\tau \simeq 0.01$), implying that practically no contrast correction is necessary to apply the model. Results for calibrated discs of diameter ranging from 20 to 700 µm are shown in figure 9. The equivalent pixel size of the imaging system is $p_o \simeq 3$ µm. The

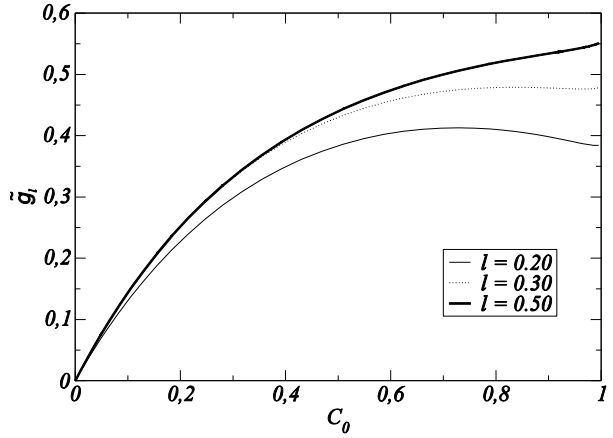

Figure 8 Dimensionless gradient as a function of the normalized contrast for relative levels $l = 0.20$, $l = 0.30$, $l = 0.50$.

maximum absolute error ($\simeq 10\ \mu m$) is obtained for the disc of 20 µm positioned near the objective ($z \simeq -0.6$ mm). The perspective effect causing change of the magnification over the range of out-of-focus positions is responsible of the large error for small objects. The error for 20 µm disc reduces to -1 µm/+3 µm (which is of the order of the pixel size) for the limited range of out-of-focus positions selected by the focus selection criterion (see below). Under these conditions, the relative error is about 6% for diameter of 60 µm, 3% for diameter of 100 µm, and of the order of 1% for diameters over 200 µm.

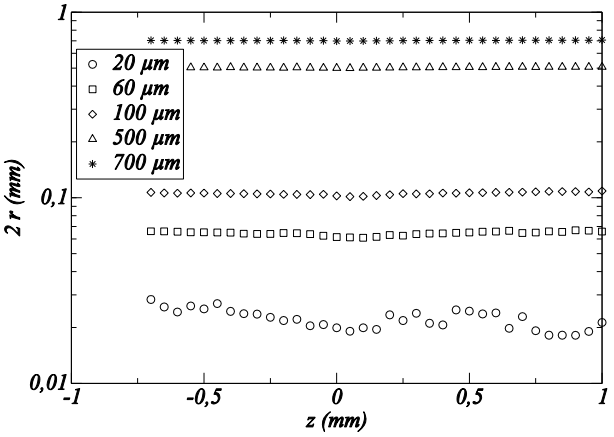

Figure 9 Sizing procedure applied to calibrated opaque discs.

PSF calibration

The PSF calibration consists in measuring the PSF half-width χ on objects precisely located in the field of view. An example of calibration with PSF half-width measured on calibrated discs is shown in figure 10. Out-of-focus aberration that is proportional to the distance from the in-focus plane (geometrical optics) plays an important role on the PSF. Thus, the variation of the PSF half-width with the distance to the in-focus plane shows a particular V-shape, resulting from the linear dependence of χ with z. The minimum PSF width is about 20 µm in the focus plane and increases up to 60 µm for 1 mm out-of-focus. The non-symmetrical variation of $\chi(z)$ is due to the perspective effect mentioned above as already observed by Fdida & Blaisot [10]. The focus selection criterion is fixed here to $2\chi_{max} = 32$ µm in order to be coherent with the chosen minimum contrast (see below). This corresponds to a depth of the measurement volume equal to 0.6 mm.

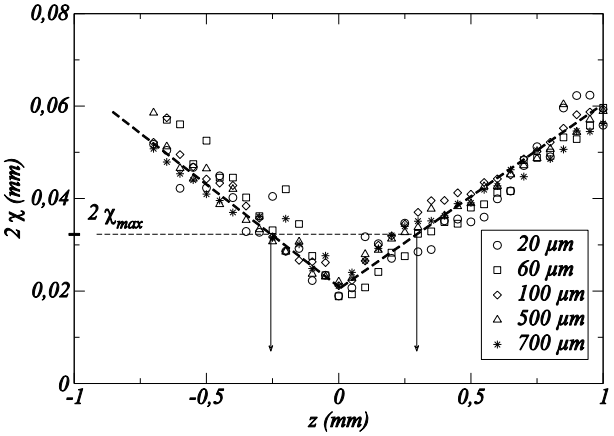

Figure 10 Variation of the PSF half-width with out-of-focus. Definition of focus selection criterion.

Effect of the reference level on sizing error

The sizing procedure is based on the measurement of the area inside an image contour. The sizing error caused by a badly determined reference level for the contour extraction is discussed here. To evaluate this error, we considered the effect of an underestimated value for l^* (noted l_u^*) on the model prediction. A too low value for l^* results in an underestimation of the size (see figure 3). The relative error $\frac{r_{l_u^*} - r_{l^*}}{r_{l^*}}$ depends on the actual image contrast as indicated in figure 11. The error is minimal for high contrast and the maximum absolute error is found for midrange contrast values. Considering a maximum underestimation of l^* about 10% (which imply an error on the measured contrast about 10% also) implies a maximum relative error about 7% for the sizing procedure.

Determination of the measurement depth and size ranges

The limitation in the measurement of drop comes first from the visibility of the drop images. In other words, images with a contrast lower than a given threshold C_{min} will not be detectable and thus not measurable. This threshold depends on the overall noise in the image acquisition chain. For a well settled system, C_{min} can be adjusted between 0.05 and 0.1. Owing to the relation between $\tilde{a}$ and C_0 shown in figure 5, one can deduce a minimum measurable object size a_{min} from the minimum contrast C_{min} and the corresponding maximum PSF half-width χ_{max} for the focus selection criterion. For $C_{min} = 0.1$ this yields to $\tilde{a}_{min} = 0.45$, i.e. $a_{min} = 0.32\ \chi_{max}$. Indeed, increasing the measurement depth results in an increase of the minimum of the measurable diameter range. In fact, droplets with diameter lower than $2a_{min}$ are still measurable, but over a narrower depth compared to the depth corresponding to the focus selection criterion. This leads to an underestimation of the drop size distribution for diameters $d < 2a_{min}$. The minimum size corresponds to a minimum area the imaging system can determine with a sufficient accuracy. This minimum size is fixed by N_{min}, the number of pixel that is considered to be significant to form an image area and the equivalent pixel size of the system:

$$a_{min} = p_o \left(\frac{N_{min}}{\pi}\right)^{1/2} \quad (10)$$

For $p_o = 3$ µm, $N_{min} = 6$ and $C_{min} = 0.1$, the minimum measurable drop diameter is of the order of 10 µm and $\chi_{max} \simeq 16$ µm (see figure 10). The maximum diameter directly depends on the detector definition and is thus connected to the field of view. As partially imaged drop cannot be measured, the effective dimensions of measurement field are given by the field of view, diminished by a frame of width equal to the radius of the biggest droplet image. Thus, in order not to reduce too much this measurement zone, the maximum diameter must be given a reasonable value, say, around 20% of the height of the field of view. For the high definition CCD used here (4000 x 2600 pixels), the maximum diameter is about 1.5 mm.

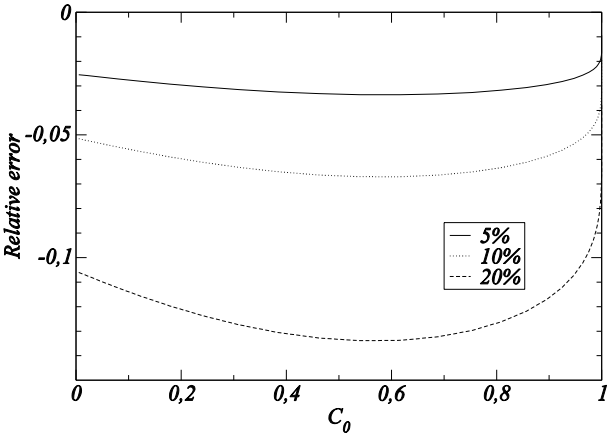

Figure 11 Relative error of the sizing procedure by underestimating the reference level I^*.

Non-uniform background and noise

The non-uniform background illumination is often an issue when dealing with backlight images of sprays. Only linear response imaging devices are considered here (no gamma-correction applied), thus the fraction of transmitted light is assessed through a normalization operation expressed by equation (11):

$$\tilde{I}(i,j) = \beta \frac{I(i,j) - I_{noise}(i,j)}{I_{back}(i,j) - I_{noise}(i,j)} \quad (11)$$

where (i,j) designate the pixel coordinates, I is the spray image, I_{back} is the background image (obtained without any object in the view field) and I_{noise} is the black noise image (obtained with the camera objective closed). Coefficient β $(0 < \beta < 1)$ is used to compensate shot-to-shot fluctuation of the light source (see Blaisot & Yon [11] for details). Subtraction of black noise is necessary for numerical signal to be effectively proportional to incoming light and for $\tilde{I}$ to correspond to the fraction of transmitted light. Non-uniform background distribution is corrected by this normalization procedure, and the resulting image profile $\tilde{I}$ takes a form similar to $\tilde{\imath}$ (as shown in figure 2). However, local background level $I_{back}(i,j)$ must remain over a given value to guarantee a minimum dynamic of the normalized signal. An acceptable value can be given by half the maximum background level. Thus, largely varying backgrounds must be avoided to keep high enough signal-to-noise ratio in normalized images.

Image segmentation - detection procedure

The segmentation is an important stage of the image processing procedure. It determines the set of droplets that will be actually analyzed. We developed a two-step segmentation based on the application of a global thresholding of the normalized image and a specific segmentation based on localization of curved grey level profiles through the use of wavelet transforms (see [11] for a more detailed explanation). This two-step segmentation can detect almost all droplets in normalized images, even the very small ones with contrast as low as 0.05, thus preventing droplet selection to depend on drop size.

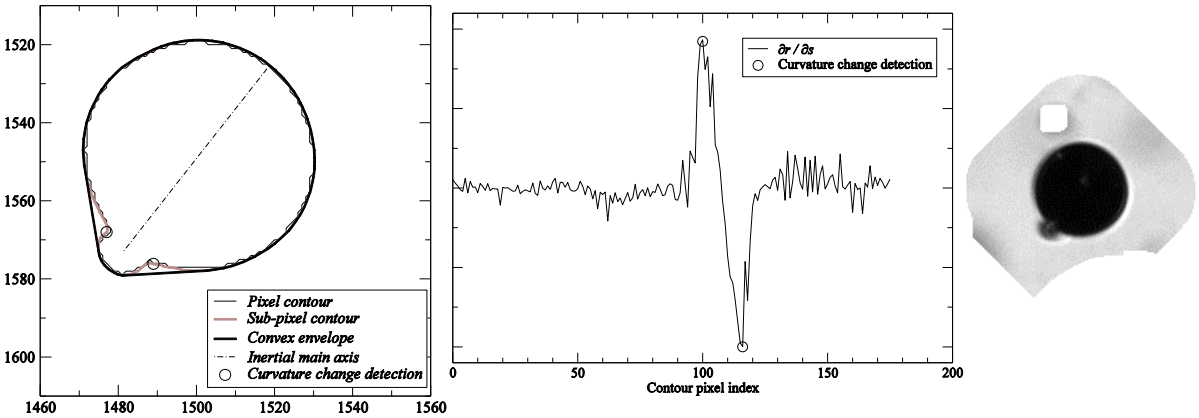

Figure 12 Image of a non-spherical object. Pixel and sub-pixel contours, as well as convex envelope and inertial main axis of the sub-pixel contour are plotted on the left. Curvature changes are localized on derivation of the distance to the object barycentre relatively to the curvilinear abscissa of sub-pixel contour.

Sub-pixel contour extraction

The sizing accuracy and the shape analysis strongly depend on contour refinement. The sizing procedure is initially based on the counting of pixels of the binary image and is enhanced by considering the grey level profile over the drop image outline. This way, finest size estimation and shape analysis are achieved as can be seen in figure 12. The sub-pixel contour is composed of the same number of points than the pixel contour. Each sub-pixel point corresponds to a point close to the pixel point, whose grey level is strictly equal to the reference level i_{l^*}. Its location is deduced from local grey level 2D linear interpolation. Real-coordinate contour is thus analyzed as a curve in a continuous space described by a limited set of points. Size and shape parameters determined from sub-pixel contours do not present discrete values any more, even for the smallest droplets.

Total and partial image overlap

Local background illumination reduction can occur in case of a drop image totally overlapped by out-of-focus drops. However, the local background level is used to compute image parameters which are thus determined as if the light source had its intensity locally reduced. In these conditions, drop sizing is still possible as soon as the local background level is high enough (see above). The problem of partially or totally overlapped droplet images was already addressed by the author [13]. It was shown that total overlapping effect is negligible on the drop size distribution as soon as the drop size can be measured on the image, i.e. as soon as 2D density projection is not too high to prevent drop contour detection. Partially overlapped droplet images (as shown in figure 12) are detected from the analysis of the contour shape. The distance from barycenter of the contour point *r* is derived relatively to the curvilinear abscissa of the sub-pixel contour *s*. Changes in contour curvature are localized from extremum points in $\frac{\partial r}{\partial s}$ (see center of figure 12). Indeed, object contours with a regular shape are characterized by $\frac{\partial r}{\partial s} \approx 0$ as can be seen for the circular part of the contour in figure 12. To complete this overlap detection, changes in grey level gradient at curvature change locations are also considered.

Summary and Conclusions

Recent advances on a drop sizing technique based on image model has been presented. The way spray drop images must be analyzed to determine drop size and shape, as well as elements for correctly settling the optical setup have been presented. Drop sizing criterion and focus selection criterion based on the model enable measurement of drop size to be achieved (within ≈ 5% error) over a controlled DOF. The sizing error is found to be about the pixel size ($p_o \simeq 3$ µm). It is shown that for application to drop size distribution measurement, focus selection criterion and lowest drop size are related to comply with the performances of the optical setup. Sub-pixel contours are used to reduce sizing error, to enhance shape analysis performances and also to detect partial overlapped droplet images.

References

[1] Fantini, E., Tognotti, L., and Tonazzini, A., *Computers and Chemical Engineering* 14: 1201-1211 (1990).
[2] Lecuona, A., Sosa, P. A., Rodriguez, P. A., and Zequeira, R. I., *Measurement Science and Technology* 11: 1152-1161 (2000).
[3] Kashdan, T., Shrimpton, J. S., and Whybrew, A. *Particle and Particle Systems Characterization* 20: 387-397 (2003).
[4] Putkiranta, M., Eloranta, H., Alahautala, T., and Saarenrinne, P., *International Symposium on Flow Visualization*, Nice, France, July 1-4, 2008.
[5] Koh, K. U., Kim, J. Y., and Lee, S. Y., *Atomization and Sprays*, 11: 317-333 (2001).
[6] Kim, K. S., and Kim, S. O., *Atomization and Sprays*, 4: 65-78 (1994).
[7] Lebrun, D., Touil, C. E., and Ozkul, C., *Applied Optics*, 35: 6375-6381 (1996).
[8] Ow, C. S., and Crane, R. I., *International Journal of Heat and Fluid Flow*, 2: 47-53 (1980).
[9] Nishino, K., Kato, H., and Torii, K., *Measurement Science and Technology*, 11: 633-645 (2000).
[10] Fdida, N., and Blaisot, J. B., *Measurement Science and Technology*, 21: 025501 (2010).
[11] Blaisot, J. B., and Yon, J., *Experiments in Fluids*, 39: 977-994 (2005).
[12] Fdida, N., Blaisot, J. B., Floch, A., and Dechaume, D., *Atomization and Sprays*, 20: 141-162 (2010).
[13] Yon, J., Blaisot, J. B., "Spray Sizing by imaging : Focusing and droplet image superposition", *19th Annual Meeting of ILASS (Europe)*, Nottingham(UK), 6-8 September.
[14] Pentland, A. P., *IEEE Transaction on Pattern Analysis and Machine Intelligence*, 9: 523-531 (1987).
[15] Ren, K. F., Lebrun, D., Ozkul, C., Kleitz, A., Gouesbet, G., and Gréhan, G., *Particle and Particle Systems Characterization*,13: 156-164 (1996).
[16] Hovenac, E. A., *Flow and Particles Diagnostics Proceedings*, 58:129–134, (1986).
[17] Goodman, J. W., *Introduction to Fourier optics*, McGraw Hill, New York (1968).